Journal of Materials Chemistry

Cite this: *J. Mater. Chem.*, 2012, **22**, 21065

www.rsc.org/materials

PAPER

Controlled synthesis of uniform magnetite nanocrystals with high-quality properties for biomedical applications†

Gorka Salas,*[ab] Cintia Casado,[a] Francisco J. Teran,[ac] Rodolfo Miranda,[ad] Carlos J. Serna[b] and M. Puerto Morales[b]

Received 6th July 2012, Accepted 16th August 2012
DOI: 10.1039/c2jm34402e

Uniform iron oxide magnetic nanoparticles, with sizes in the range 9–22 nm, have been synthesized by thermal decomposition of an iron oleate complex in 1-octadecene, controlling reaction parameters related to the nucleation and growth processes. After transferring to water through a ligand substitution process, nanoparticles display very good magnetic and magneto-thermal properties. The relationship between these properties and the size and size distribution of the particles is discussed. The colloidal stability of the nanoparticles dispersed in common biological buffers has also been studied.

Introduction

The synthesis of iron oxide nanoparticles (IONPs) has been intensively developed in the last few years because of their technological interest for biomedical applications, energy storage devices (anodes for lithium ion batteries), photoelectrochemical water splitting and other forms of catalysis.[1] Physico-chemical properties of the nanoparticles are strongly affected by their size, shape and crystalline structure. Numerous methods have been reported to produce uniform nanoparticles with well defined size and shape, including those using surfactants, micelles or dendrimers among others.[2]

The high-temperature decomposition of an iron organic precursor using surfactants and organic solvents is one of the best methods to produce highly monodisperse IONPs, allowing size control in the range between 4 and 15 nm.[3–5] The most common procedure for this synthesis is the one reported by Sun and Zeng,[4] using $Fe(acac)_3$ (acac = acetylacetonate) as the iron source in the presence of oleic acid, oleylamine and 1,2-hexadecanediol, in a solvent with a high boiling point. Data suggested that an intermediate iron oleate complex is formed *in situ* during the reaction playing an important role in the formation of the nanoparticles.[3b,6] Indeed, large IONPs (15–20 nm) with good size control, although low magnetization, have been obtained by directly using an iron(III) oleate complex as a precursor.[7] Seed-growth methods have also been employed[3a,4] to increase the IONP size with some drawbacks like structural defects in detriment of the IONPs' magnetic properties.[8]

Thermogravimetric analysis (TGA) and differential scanning calorimetry (DSC) have been used to explore the mechanism of the reaction, leading to different interpretations.[7,9,10] It has been reported that nucleation takes place at 200–240 °C by dissociation of one oleate ligand and CO_2 elimination, while slow nanoparticle growth begins at $T > 250$ °C but occurs mainly at *ca.* 300 °C after dissociation of the remaining two oleate ligands from the precursor.[7] Larger IONPs were obtained when increasing the reaction temperature or the amount of oleic acid added to the reaction medium. In another work, the following was proposed: a first step at 150–230 °C, involving dissociation of two oleate ligands, and a second one at 230–295 °C, related to the dissociation of the third oleate, both steps being accompanied by CO_2 release.[9] Nevertheless TGA/DSC data must be cautiously taken, given that such analyses are performed over the isolated iron oleate complex, while the synthesis of IONPs is accomplished in an organic solvent dispersion and in the presence of other reagents such as oleic acid.

Reports concerning the synthesis of iron oxide nanoparticles by thermal decomposition are not always clear, or do not provide enough information, about experimental procedures for obtaining IONPs with uniform size distribution and control of the morphology. For example, data found in the literature are sometimes contradictory concerning the issue of how the amount of stabilizer affects the size and shape of the IONPs, as it has been recently highlighted.[11] In addition it is not always indicated whether the reaction was carried out with or without stirring, magnetically or mechanically, or if it was performed under a nitrogen atmosphere or not. The stirring issue is very important

[a]*Instituto Madrileño de Estudios Avanzados en Nanociencia, Campus Universitario de Cantoblanco, 28049 Madrid, Spain. E-mail: gorka.salas@imdea.org*
[b]*Instituto de Ciencia de Materiales de Madrid, ICMM-CSIC, Sor Juana Inés de la Cruz 3, Campus Universitario de Cantoblanco, 28049 Madrid, Spain*
[c]*Unidad Asociada de Nanobiotecnología, CNB-CSIC & IMDEA Nanociencia, Campus Universitario de Cantoblanco, 28049 Madrid, Spain*
[d]*Departamento de Física de la Materia Condensada and Instituto Nicolás Cabrera, Universidad Autónoma de Madrid, Campus Universitario de Cantoblanco, 28049 Madrid, Spain*

† Electronic supplementary information (ESI) available: Additional data for the characterization of the iron oleate complex and IONPs, as well as a table summarizing the main features of IONPs. See DOI: 10.1039/c2jm34402e

because of the heterogeneous nature of this kind of reaction given that: (i) it usually involves one to four reagents in relatively high concentrations (*ca.* 0.1 M); (ii) molecular species can coexist with *in situ* formed nuclei, especially at the beginning of the reaction; and (iii) small and larger nanoparticles can be present at the same time in proportions depending on the separation of nucleation and growth stages. Under these conditions mass transfer plays an important role; so the stirring of the reaction mixture is critical.

The magnetic properties of IONPs obtained by this method are, obviously, of utmost importance, although they are not always described in the literature. Low saturation magnetization values, typically below 60 emu g^{-1} and sometimes even lower than 30 emu g^{-1}, have been reported for magnetite particles.[7,12–15] Surprisingly, this problem specially affects larger particles (10–25 nm).[7] One reason for this could be the unnoticed presence of smaller nanoparticles or the undesired formation of wüstite (FeO), an iron oxide phase different from Fe_3O_4 and γ-Fe_2O_3. This wüstite phase has been observed in IONPs synthesized by thermal decomposition of an iron oleate precursor.[11] Furthermore, it has been demonstrated that it is possible to deliberately synthesize wüstite nanoparticles by thermal decomposition of iron oleate and iron acetylacetonate.[16,17] Seed-growth methods do not overcome the problem of low magnetizations in IONPs with core sizes > 10 nm,[3a] with internal defects accounting for the reduction in magnetisation.[8]

Therefore, the improvement of the crystallinity and uniformity of large (>10 nm) magnetite nanoparticles prepared by thermal decomposition of organic precursors to obtain good magnetic response, crucial for some applications like magnetic hyperthermia,[18] is still a challenge and is one of the goals of the work presented in this paper.

In the first part of this work we try to shed some light on the effects of different synthesis parameters on the resulting material in order to rationalize this process and make it reliable. We study the formation of magnetic IONPs by thermal decomposition of an iron coordination complex, $Fe(oleate)_3$, in 1-octadecene, an organic solvent with high boiling point (*ca.* 315 °C). The material obtained is composed of magnetite (Fe_3O_4) and/or maghemite (γ-Fe_2O_3). The effects of different experimental parameters on the IONPs size, size distribution, shape and magnetic and magneto-thermal properties have been analysed varying the stabilizer concentration (oleic acid or oleic acid and oleylamine), the stirring and the reaction time.

The obtained nanoparticles are hydrophobic while any potential use in biomedical applications requires nanoparticles dispersed in physiological media. Therefore, in the second part of the present work, we describe the surface modification of the nanoparticles through a ligand substitution process with *meso*-2,3-dimercaptosuccinic acid (DMSA) that yields hydrophilic DMSA-coated nanoparticles very stable in water dispersions. The magnetic properties of the IONPs dispersed in water have been studied, finding that they are superparamagnetic at room temperature and preserve relatively high saturation magnetization values.

The stability of the IONPs dispersed in water or in biological buffers has been studied, concluding which is the best way to handle the nanoparticles prior to *in vivo* or *in vitro* experiments. We have also studied the influence of different parameters (nature and concentration of the buffer, IONP concentration and core size) on the colloidal stability, and identified the main source of stability for DMSA-coated nanoparticles.

DMSA-coated IONPs have been proven to be internalized by diverse cancer cell lines.[19–21] They are active as contrast agents for magnetic resonance imaging,[20] or as drug carriers against pancreatic tumour in animal models.[21] Superparamagnetic nanoparticles are able to generate heat when being exposed to alternating magnetic field (H_{AC}). Thus, another potential biomedical application of IONPs is to use this dissipation power as a therapeutic approach against cancer.[22] This subject is currently the object of big efforts in nanobiomedical research.[23] The physical magnitude employed to evaluate the magneto-thermal properties of IONPs is the mass-normalized specific absorption rate (SAR).[22] In the last part of the article the SAR values of some of the IONPs are shown and discussed. Our results highlight the importance of the size, and size distribution, of magnetic IONPs in the heat generation efficacy.

Experimental part

Reagents and materials

Commercial products iron(III) chloride hexahydrate (≥98%, Sigma-Aldrich), sodium oleate (≥82%, Riedel-de Haën), oleic acid (90%, Aldrich), oleylamine (70%, Aldrich), *meso*-2,3-dimercaptosuccinic acid (DMSA, 98% Aldrich), 1-octadecene (90%, Aldrich), *n*-hexane (99%, Scharlau), toluene (99.8%, Sigma-Aldrich), dimethyl sulfoxide (>99.5%, Sigma-Aldrich), ethanol (96%, Panreac) and phosphate buffered saline solution PBS 10× (tested for cell culture, Sigma) were used as received. Dialysis tubing cellulose membranes were purchased from Sigma and washed prior to use.

Characterization

Fourier transform infrared measurements (FT-IR) were carried out in a Nicolet 20SXC FT-IR spectrometer. Samples were dispersed in KBr at 2 wt% and pressed in a pellet. The IR spectra were registered between 4000 and 400 cm^{-1}.

^{13}C cross-polarized magic angle spinning nuclear magnetic resonance (^{13}C CP MAS NMR) spectra were obtained in a Bruker Avance 400 spectrometer, using a standard cross-polarization pulse sequence. Samples were spun at 10 kHz. Spectrometer frequencies were set to 100.62 and 400.13 MHz for ^{13}C and ^{1}H respectively. A contact time of 2 ms and a period between successive accumulations of 4 s were used. The number of scans was 400 for sodium oleate and 14 800 for the iron oleate complex. Chemical shifts (in ppm) were referenced to TMS.

The Fe content in the samples was determined by inductively coupled plasma-optical emission spectrometry (ICP-OES, PerkinElmer Optima 2100 DV ICP) after dissolving the samples in HNO_3 : HCl 1 : 3 mixtures and diluting them with doubly distilled water.

Simultaneous thermogravimetric/differential thermal analysis (TGA/DTA) of the samples was carried out in a Seiko Exstar 6300 instrument. For this analysis, a heating rate of 10 °C min^{-1} in air atmosphere from room temperature to 1000 °C was applied to the sample.

Particle size and shape were examined by transmission electron microscopy (TEM; 200 keV microscopes JEOL JEM 2000 FXII, ICMM-CSIC, and JEOL JEM 2100, ICTS-CNME). Samples were prepared by placing one drop of a dilute suspension in hexane onto a carbon coated copper grid and leaving it to dry at room temperature. The size distributions were determined through manual analysis of ensembles of over 300 particles found in randomly selected areas of the enlarged micrographs, with Imagetool software to obtain the mean size and standard deviation. High resolution TEM (HRTEM) images were obtained by means of a Philips TECNAI 20 (Centro de Apoyo Tecnológico, Universidad Rey Juan Carlos).

The hydrodynamic size (D_{HYD}) was measured by dynamic light scattering (DLS) from a dilute suspension of the sample in water at pH 7 in a standard cuvette, using a Zetasizer NanoZS device (Malvern Instruments). The energy source was a laser emitting green light, and the angle between the sample and detector is 173°. D_{HYD} in this work will refer to the *Z*-average size, since this is the most reliable value produced by the DLS technique.

Magnetic characterization of aqueous suspensions (100 μL) were carried out in a vibrating sample magnetometer (VSM; MLVSM9 MagLab 9 T, Oxford Instrument). Magnetization curves were recorded at 250 and 5 K by first saturating the sample in a field of 5 T. M_S was evaluated by extrapolating to infinite field the experimental results obtained in the high field range where the magnetization linearly increases with $1/H$. ZFC/FC data were obtained by first cooling the sample in zero applied field (ZFC process) from room temperature to $T = 5$ K. Then, a field of $H = 100$ Oe was applied and the variation of magnetization was measured while increasing the temperature up to $T =$ 260 K. After the last point was measured, the sample was cooled again to $T = 5$ K keeping the same field (FC process) and the magnetization was again measured while increasing the temperature.

The specific absorption rates of water dispersed IONPs have been determined with high accuracy by non-adiabatic calorimetric measurements, as reported elsewhere.[24] For the present study, calorimetric measurements have been performed on IONPs dispersed in water with an iron concentration of 10 g L^{-1} and using a reduced volume of 30 μL subjected to given H_{AC} conditions (50 mT and 77 kHz during 8 minutes) at equilibrium temperatures near 28 °C. The sample holder is a glass flask with a vacuum shield covered by a polystyrene stopper where an upper aperture allows introducing the temperature probe. This aperture is responsible for the thermal exchange between the sample and the surroundings (laboratory environment) *via* convection mechanisms. The use of reduced volume makes radiation thermal exchange negligible.[24] H_{AC} up to 250 kHz and 50 mT are generated by a home-made air-cooled ferrite core coiled with Litz wires, which is part of a LCR resonant circuit. The temperature evaluation of water dispersed IONPs exposed to H_{AC} was done with a commercial optical fibre probe TS2/2 connected to a FOTEMP2-16 two-channel signal conditioner from Optocon AG with an experimental error of ±0.2°C. Mass-normalized SAR values were obtained by modelling the temperature variation curves of IONPs measured in our experimental set-up of controlled heat losses in order to increase the SAR accuracy.[24]

Synthesis

Synthesis of the iron oleate complex. The synthesis was done by slight modification of a previously described procedure.[7] $FeCl_3 \cdot 6H_2O$ (10.8 g, 40 mmol) and an excess of sodium oleate (minimum purity 82%, 45 g, >120 mmol) were dissolved in a mixture of water (60 mL), ethanol (80 mL) and hexane (140 mL) obtaining a biphasic system composed of a deep red solution (up) and a colourless and transparent phase (down). The reaction mixture was heated to reflux (70 °C) for 4 hours, with vigorous magnetic stirring. Then the system was allowed to cool down to room temperature. The aqueous phase (pale yellow) was separated and discarded and the organic phase (dark red) was washed with water–ethanol mixtures (4 × 50/10 mL). The organic solvents were removed in the rotavapor resulting in a dense and oily product that was dried in the oven at 50 °C for 3 days. The obtained iron oleate complex is a waxy reddish-brown product.

Synthesis of iron oxide nanoparticles under stirring. The reaction was carried out under nitrogen. In a round-bottomed flask of 0.5 L, equipped with a mechanical stirrer (PTFE centrifugal stirrer shaft, Ø = 75 mm) thermometer, entry for nitrogen flow and reflux condenser, iron(III) oleate (4.5 g, 5 mmol) was mixed with oleic acid and, if indicated, oleylamine (see Table 1 for amounts) in 1-octadecene (50 mL). The mixture was stirred (100 rpm) and slowly heated (2 °C min^{-1} for $T < 100$ °C, and 3 °C min^{-1} for $T > 100$ °C) until reflux (315 °C) with a heating mantle. After one hour at that temperature the heating mantle was withdrawn and the system was allowed to cool down to room temperature. The resulting black mixture was washed with ethanol (10 × 40 mL), centrifuged (RCF = 9000), and the particles separated with the aid of a magnet. The resulting black solid was redispersed in hexane for long-term storage.

Table 1 Reaction conditions in the synthesis of IONPs under stirring. All the reactions were carried out under nitrogen, with mechanical stirring (100 rpm), and were kept for 1 hour at 315 °C

Entry	Label	[Fe(oleate)$_3$] (mol L^{-1})	Oleic acid (mol L^{-1})	Oleylamine (mol L^{-1})	Mean size[a] (nm)	Shape
1	IO-1	0.1	—	—	9 ± 2	Spherical polyhedra
2	IO-2	0.1	0.05	—	12 ± 1	Spherical polyhedra
3	IO-3	0.1	0.1	—	9 ± 1	Spherical polyhedra
4	IO-4	0.1	0.15	—	9.5 ± 0.8	Spherical polyhedra
5	IO-5	0.1	0.3	—	8.9 ± 0.8	Spherical polyhedra
6	IO-6	0.1	0.05	0.05	18 ± 4	Octahedral

[a] Mean size and standard deviation as measured by TEM.

Table 2 Reaction conditions in the synthesis of IONPs without stirring. $[Fe(oleate)_3] = 0.1$ M [oleic acid] = 0.05 M

Entry	Label	Reaction time (hours)	Mean size[c] (nm)
1[a]	IO-7	1	15 ± 4
2[b]	IO-8	1	14 ± 1
3[b]	IO-9	2	18 ± 2
4[b]	IO-10	3	22 ± 2

[a] No stirring at all. [b] Reaction stirring only until 50 °C to ensure a homogeneous mixture. [c] Mean size and standard deviation as measured by TEM.

Synthesis of iron oxide nanoparticles without stirring. Samples IO-8, IO-9 and IO-10 (see Table 2 for labels) were synthesized by the previous procedure, but stopping the stirring at 50 °C. IO-7 was synthesized without any stirring at all.

Transfer to water through ligand substitution with DMSA

In a typical experiment, ethanol (20 mL) was added to a volume of IONPs dispersed in hexane containing a mass of Fe_3O_4 of 50 mg. The mixture was sonicated and then placed on a magnet to separate the liquid from the black solid residue of nanoparticles. The residue was washed with more ethanol (5 × 10 mL) following the same procedure, until the discarded liquid had a clean appearance. The remaining black residue was dispersed in toluene (20 mL) and the dispersion added to a solution of DMSA (90 mg) in dimethyl sulfoxide (5 mL). The resulting black suspension was then shaken in a laboratory tube rotator. After 2 days, DMSA-coated nanoparticles were precipitated as a black powder stuck to the glass tube and the liquid phase was transparent and pale yellow. The liquid was discarded and the nanoparticles were washed with ethanol (4 × 10 mL), sonicating and centrifugating (RCF = 9000). The final black solid was air dried and redispersed in distilled water. $NaOH_{(aq)}$ was added to increase the pH from *ca.* 3 to 10. The dispersion was then placed in a cellulose membrane and dialyzed for 4 days in distilled water, to remove any excess of unreacted DMSA and any other small impurities that may be present in the dispersion without being attached to the nanoparticles. Finally the pH of the dispersion (*ca.* 5) was adjusted to 7 and the dispersion filtered through a polyethylene oxide filter with a pore size of 0.22 μm. This avoids bacteria or dust in the final dispersion. It is worth noting that this last step of sterilization by filtration is not necessary if the nanoparticles are not going to be used for biological purposes.

Study of the stability of IONPs in PBS buffer

Samples were diluted with distilled water and commercial PBS 10× buffer (Sigma, NaCl 1.54 M and 100 mM in phosphates) in order to match the studied iron concentrations (0.5, 0.1 and 0.05 g L^{-1}) and the corresponding buffer concentrations. *[PBS1x]*, *[PBS1x]*/2, *[PBS1x]*/4 and *[PBS1x]*/8 refer to samples in which the commercial PBS 10× buffer has been diluted 10, 20, 40 and 80 times. Samples with only NaCl or phosphates (Na_2HPO_4 and NaH_2PO_4) were prepared in a similar manner but dissolving the necessary amount of the corresponding salt.

Results and discussion

Synthesis and characterization of the iron oleate precursor

Iron(III) oleate, $Fe(oleate)_3$, was synthesized by slight modification of a previously published method (see Experimental part for details).[7] The importance of the work-up of the reaction has been previously stressed, as the obtained iron oleate may display different structures than $Fe(oleate)_3$ depending on the washing and drying steps.[10] The chemical nature of the iron precursor has considerable influence on the properties of the obtained nanoparticles. For this reason, an excess of sodium oleate has been used in this work to ensure completion of the reaction to obtain $Fe(oleate)_3$. The complex has been characterized by FT-IR, ^{13}C CP MAS-NMR, TGA/DTA and ICP-OES.

The FT-IR spectrum of the iron(III) oleate complex is shown in Fig. S1.† The asymmetrical, $\nu_a(COO^-)$, and symmetrical, $\nu_S(COO^-)$, stretching bands of the carboxylate group appear at 1575 cm^{-1} and 1450 cm^{-1} respectively.[25] The difference between both (125 cm^{-1}) fits well with the oleate being coordinated to iron as a bidentate (chelate) ligand, as depicted in Scheme 1).[10,25] However, the band at 1725 cm^{-1} makes it difficult to distinguish if the three oleates are acting as bidentate ligands or if there are one or two monocoordinated oleates.

To shed more light on the real structure of the iron oleate complex, it has been studied by ^{13}C CP MAS-NMR (Fig. S2†). In the NMR spectrum of the complex the signal from the carboxylic carbon is missed, which is not strange for quaternary carbons in CP MAS experiments.[26] Nevertheless, the adjacent methylene carbon appears at 57.1 ppm, clearly shifted downfield if compared with the same carbon in the spectrum of the ionic sodium oleate (38.5 ppm, Fig. S2†), indicating the coordination of the oleate ligand to the iron atom. No other signals arising from the same carbon can be observed, as it would be the case if the oleate were bound to the metal by different coordination modes. This result suggests that the iron oleate structure is well represented by the one depicted in Scheme 1.

The iron content of the iron oleate, determined by ICP-OES, is 6.7% in weight, which is close to the theoretical value of 6.2% for $Fe(oleate)_3$.

To get further information about the iron complex precursor and its thermal behaviour, TGA/DTA analysis of the product was performed. Initially, mainly between 315 °C and 355 °C (region A–B in Fig. S3†), there is a weight loss of 30%, which is coherent with the loss of one oleate ligand. A second step (~25% weight loss) takes place roughly between 355 °C and 400 °C (region B–C in Fig. S3†) followed by a final step of ~45% weight loss at higher temperatures (region C–D in Fig. S3†). These three

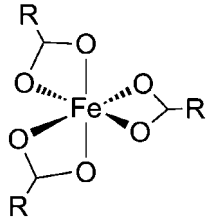

Scheme 1 Iron(III) tris(oleate) synthesized in this work for the synthesis of IONPs. $R = -(CH_2)_7-CH{=}CH-(CH_2)_7-CH_3$.

steps account for the loss of the three oleate molecules and no significant weight change is observed over 470 °C. The final residue consists of α-Fe_2O_3 and represents 9.7% of the total weight of the initial sample. This implies that the sample contains 6.8% in weight of Fe. This iron content fits almost perfectly with the one measured by ICP-OES for the complex $Fe(oleate)_3$. As stated in the introduction, thermal analysis has been previously used to study the mechanism of the nanoparticle formation from an iron oleate precursor.[7,9,10] However, caution must be taken when interpreting such data in terms of the temperature for oleate release and complex decomposition, because thermal analyses are performed on solid samples, while the synthesis of the nanoparticles is accomplished in an organic solution or dispersion.

Synthesis of IONPs by thermal decomposition in 1-octadecene

The synthesis of iron oxide magnetic nanoparticles has been carried out by thermal decomposition of the $Fe(oleate)_3$ precursor in 1-octadecene, by modifications of a previously reported procedure (see Experimental section).[7] This procedure leads to IONPs mainly composed of a mixture of magnetite (Fe_3O_4) and maghemite (γ-Fe_2O_3), with a higher proportion of the former in larger IONPs.[7] Reactions were carried out with and without stirring (Tables 1 and 2 respectively) and in the presence of different amounts of oleic acid and oleylamine as stabilizers (Table 1).

Data show a complex relationship between particle size and the amount of oleic acid added, without very large variations (Fig. 1 and black squares in Fig. 2). A qualitatively similar behaviour has been previously observed, although no explanation was brought forward by the authors.[11] Other reports however describe different relationships between the nanoparticle size and the amount of stabilizers. For example, it has been reported that, with $Fe(acac)_3$ as the iron precursor, the size of the IONPs tends to decrease[27] or increase[28] when the amount of surfactant (oleic acid and oleylamine) increases. On the other hand, using FeO(OH) as the iron precursor, Colvin and co-workers found that the size of the IONPs increased linearly with oleic acid concentration, until reaching certain limit where nanoparticle formation is inhibited.[6] Our results show that, when increasing the amount of oleic acid added, there is first an enlargement of the IONPs followed by a reduction of the size (Fig. 2). Furthermore, the low amount of surfactant present in IO-1 (only the oleate molecules of the iron precursor, with no oleic acid added) drives to a broader size distribution (see histograms in Fig. 1 and graph in Fig. 2) that is dramatically reduced in the other samples.

To get a qualitative explanation for these results we can consider a simplified view of the reaction mechanism, as sketched in Scheme 2. For clarity, no redox reactions are considered although they certainly occur in the synthesis of Fe_3O_4 nanoparticles from Fe(III) precursors. In accordance with the classical LaMer–Dinegar mechanism, there is a first stage of nucleation followed by a second one of growth.[29] For a good size control (*i.e.* to obtain monodisperse nanoparticles), nucleation and growth must be separated. This can be achieved if: (i) nucleation and growth take place at different temperatures or (ii) nucleation

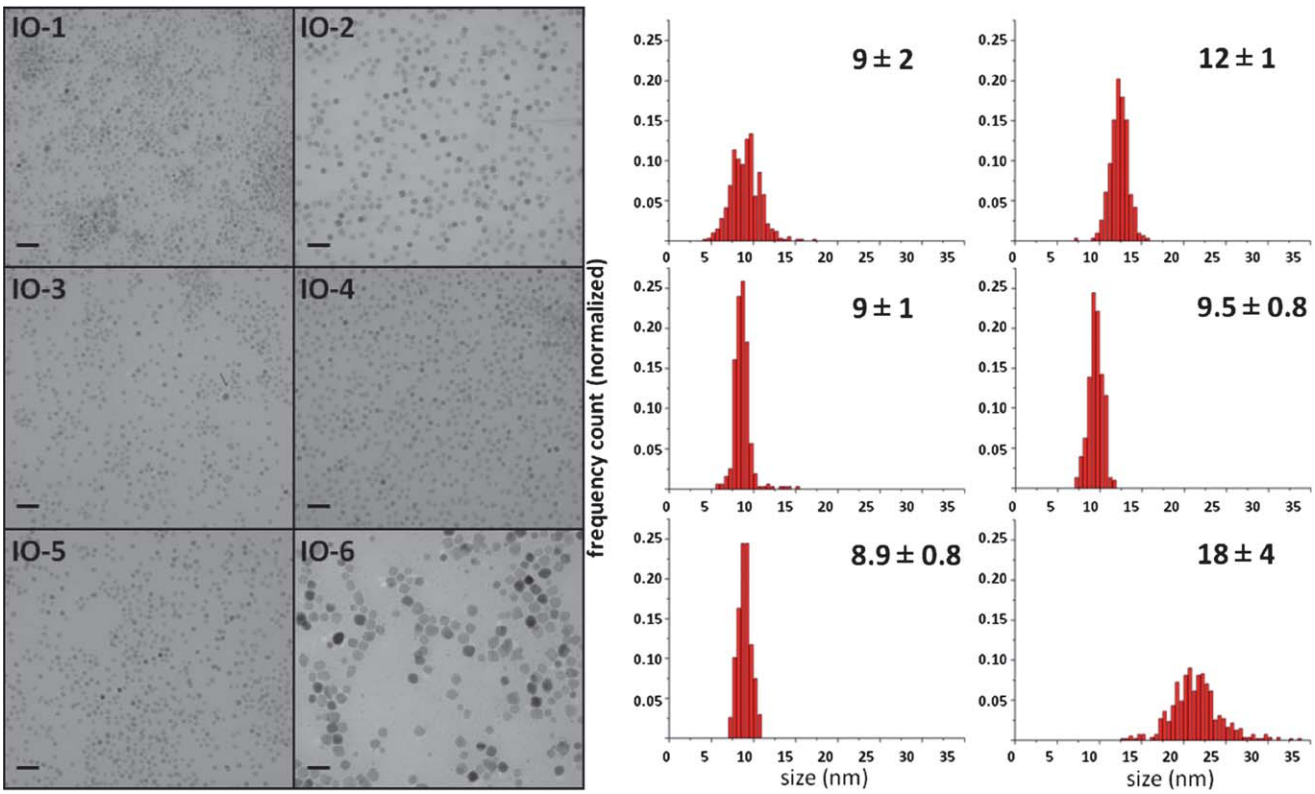

Fig. 1 Selected TEM micrographs and histograms of normalized size distributions of IONPs synthesized under stirring (see Table 1 for labels). Scale bars = 40 nm.

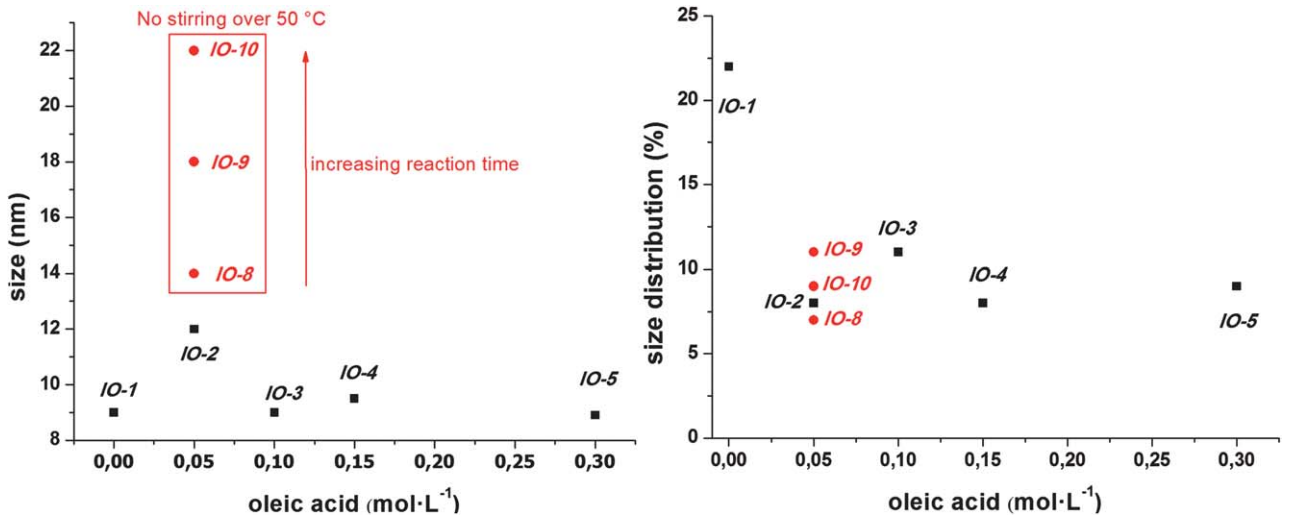

Fig. 2 Dependence of the IONP core size and size distribution (expressed as standard deviation percentage) on the concentration of oleic acid added.

and growth take place with very different rates (r_n and r_g respectively). In the synthesis of IONPs by thermal decomposition of an iron oleate precursor, as the one discussed here, it has been reported that nucleation takes place at 200–240 °C while growth mostly occurs around 300 °C. However, it is worth noting that slow growth already exists at some point in the 200–250 °C range, meaning that both processes can be overlapped.[7,9] Thus, key points of this synthesis are the reaction rates of the nucleation and growth stages, r_n and r_g respectively (see Scheme 2). If $r_n \gg r_g$ then both processes will take place separately and nanoparticles will be very homogeneous in size and shape. In addition, if r_g is very low, small nanoparticles will be obtained unless the temperature is increased enough to favour the growth process. If r_n and r_g are similar (same order of magnitude) then both stages will take place at the same time, and the nanoparticles will be generated with a poor control of the size. Both r_n and r_g also affect the mean size of the particles, and not only the size distribution, as they affect the number of available nuclei and how fast they grow.

In our case, differences in the chemical kinetics are necessarily due to differences in the concentrations of added oleic acid, which affects the nucleation and growth steps. Temperature (and temperature ramp), solvent and initial concentration of the iron oleate precursor were kept constant (Table 1). During nucleation, iron oxide nuclei are surrounded and stabilized by oleic/oleate molecules (Scheme 2). A minimum concentration of oleic/oleate is needed to ensure the stabilization of those nuclei, preventing them to undergo coalescence or aggregation as soon as they are formed. In IO-1, only the oleate molecules of the precursor are present, leading to particles with a wide size distribution (Fig. 2). On increasing oleic/oleate concentration, nucleation is hampered forming fewer nuclei but resulting in larger particle size (IO-2). The reaction can be inhibited if the concentration of oleic/oleate molecules in the medium is too high; so no nuclei will be formed and no nanoparticles will be observed.[6] On the other hand, the growth step will be faster (r_g higher) with low oleic/oleate concentrations leading to larger particles at shorter heating times. However, at high oleic/oleate molecule concentration, the growth process is slower requiring longer heating times at the maximum temperature to reach larger particle sizes (IO-3, -4, -5).

In IO-6, oleic acid and oleylamine are employed together as stabilizers (both in concentrations of 0.05 M) and large IONPs (18 ± 4 nm) are obtained (Table 1). However, the size distribution is broader under these conditions, with a relatively large proportion of small nanoparticles together with larger ones (Fig. 1), as it has been previously observed with other amine ligands.[5] No change in the size of the nanoparticles and no improvement in terms of size distribution were observed when the reaction mixture was kept for a longer time (4 hours) at the maximum temperature. Oleic acid and oleylamine act as ligands competing for the same coordination positions at the surface of

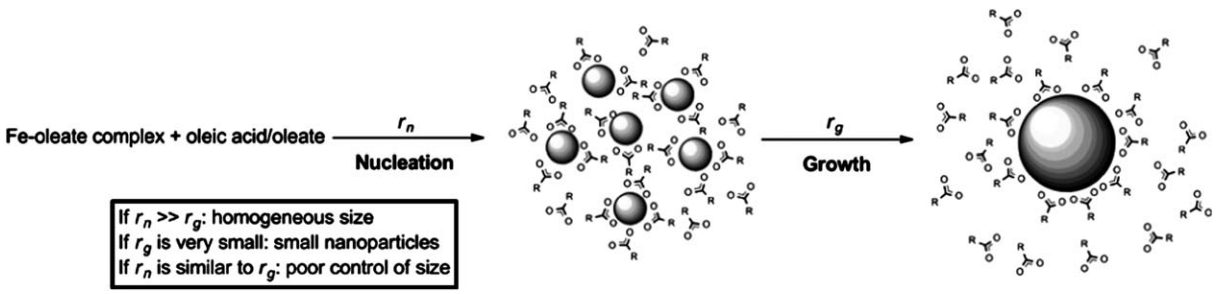

Scheme 2 Simplified view of the nucleation and growth stages during nanoparticle formation. r_n and r_g correspond to the rates of nucleation and growth, respectively.

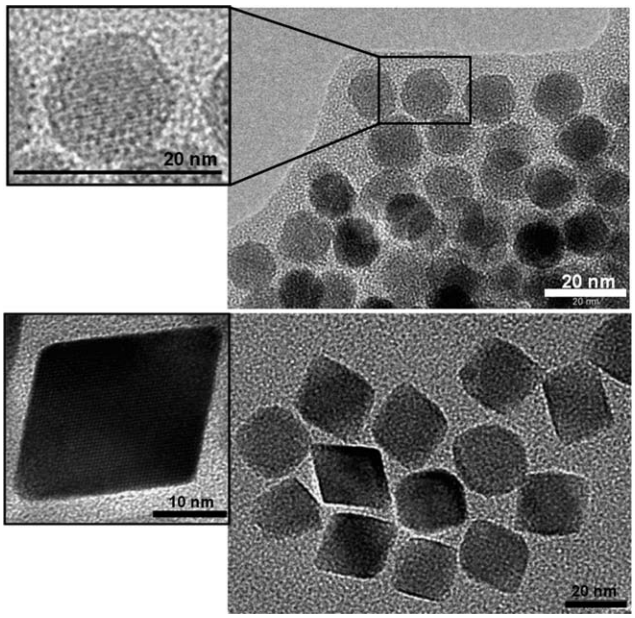

Fig. 3 Selected HRTEM micrographs of IO-2 (up) and IO-6 (down).

the nanoparticles and both are involved in equilibrium reactions between their coordinated and uncoordinated forms. As oleylamine is a worse ligand for the iron oxide surfaces than oleic acid, the equilibrium between free and coordinated ligands will be shifted towards the release of ligands to a greater extent with amines than with oleic acid, favouring the nanoparticle growth in a less controlled manner.[5]

There are also differences regarding the shape of the particles as a function of the surfactant. While IO-2 nanoparticles are almost spherical polyhedra, IO-6 nanoparticles with oleylamine display mostly octahedral or truncated octahedral shapes (see HRTEM images of IO-2 and IO-6 in Fig. 3). High resolution TEM of IO-2 and IO-6 show that IONPs are highly crystalline, even in the case of the sample less regular in shape (IO-6), as shown in Fig. 3. In IO-6, the measured distance between adjacent {111} planes is 0.48 nm and the angle between intersecting {111} planes is 70.6°, almost coincident with the theoretical value (70.5°).[30] The dominating octahedral shape in IO-6 indicates that the growth rate along the ⟨100⟩ direction was higher than that along the ⟨111⟩ direction (ratio R between both is *ca.* 1.73), leading to crystals exhibiting the most stable {111} facet.[30] Interestingly, this behaviour has also been observed in the synthesis of FeO nanoparticles by decomposition of $Fe(acac)_3$ in the presence of oleic acid and oleylamine in 1 : 1 ratio.[16] The polyhedral shapes observed in the case of particles prepared only with oleic acid (IO-2) are due to a decrease in the relative growth rate along the ⟨100⟩ direction when compared with the ⟨111⟩ ($0.58 < R < 1.15$),[30] indicating that the oleic/oleate and oleylamine ligands have different affinities for the different crystallographic planes.

The effect of the stirring on the IONP formation was investigated for a sample prepared with the same reagents in the same concentration than sample IO-2 (Table 1, entry 2). Data are displayed in Table 2.

IONPs with a mean size of 15 nm and a broad size distribution are obtained if the reaction mixture is not stirred at all (IO-7,

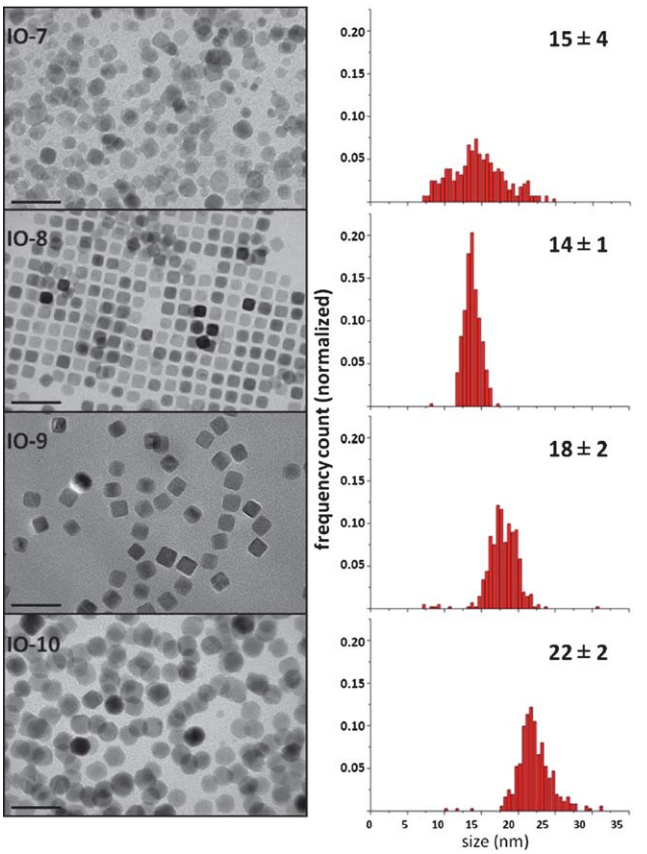

Fig. 4 TEM micrographs and normalized size distribution histograms of IONPs synthesized without stirring (see Table 2 for labels). Scale bars = 50 nm.

Table 2, entry 1; Fig. 4). The reaction mixture is highly heterogeneous from the beginning which makes it difficult to control the size and shape of the IONPs. This problem has been easily overcome by stirring the reaction at the beginning of the heat ramp, until it reaches 50 °C. This leads to a homogeneous mixture from the beginning that ends up in uniform nanocrystals (entries 2–4 in Table 2 and Fig. 4). The size of these nanocrystals has been selectively adjusted between 14 and 22 nm by just applying longer reaction times at the maximum temperature, from 1 to 3 hours. This occurs through Ostwald ripening once the iron precursor has been decomposed. Larger IONPs grow at the expense of the shrinking and dissolution of the smaller ones, resulting in IONPs very homogeneous in size and shape.[12,31]

From the TEM micrograph of IO-8 shown in Fig. 4 it is possible to measure the inter-particle distance, $d = 3.25 \pm 0.32$ nm, which is less than double of the length of one molecule of oleic acid (1.7–2 nm). This means that the surfactant must be either tilted at some degree over the surface of the nanoparticle or with part of the hydrocarbon chains on one particle interacting with that of the nearest particle.

Surface modification of the nanoparticles with *meso*-2,3-dimercaptosuccinic acid (DMSA)

IONPs generated by thermal decomposition, as those discussed here, are hydrophobic and therefore not useful for *in vitro* or *in vivo* experiments. In this work, a ligand substitution process

with DMSA has been employed to obtain nanoparticles that can be dispersed in water and in physiological media. These DMSA-coated IONPs are stable in water dispersion for several months, with hydrodynamic sizes (D_{HYD}; measured by DLS) below 70 nm in all cases. D_{HYD} values (expressed as *Z*-average sizes, Table S1†) are always higher than sizes measured by TEM, indicating some degree of agglomeration after the ligand substitution. Additionally size values based on intensity, volume and number, obtained by DLS, are shown in Fig. S6.†

This procedure (see Experimental part for details) consists of the following steps: (a) *Ligand substitution* of oleic acid by DMSA. Under these conditions a fraction of the thiol groups are oxidized forming disulfide bridges.[32] (b) *Alkalinization* to increase the surface charge and enhance the stability of the IONPs by electrostatic repulsion between the COO^- groups.[32] Thiol groups which are not involved in disulfide bridges are deprotonated at pH = 10 resulting in thiolate groups that have affinity for iron atoms and may lead to partial substitution of carboxylate moieties at the surface of the nanoparticles.[32] (c) *Dialysis* to remove any excess of unreacted DMSA and any other small impurities present in the dispersion. (d) *Sterilization* adjusting the pH to 7 and filtering through 0.22 μm to avoid the presence of bacteria or dust in the final dispersion.[33]

Infrared analysis of the DMSA-coated IONPs (Fig. S4†) does not show the S–H stretching band around 2500–2600 cm^{-1} indicating that all or almost all thiol groups have been transformed in thiolate groups or are forming disulfide bonds.

Magnetic properties

In order to evaluate the influence of the different synthetic conditions on the magnetic properties of the resulting IONPs, we have characterized their magnetic behaviour at different temperatures. Thus, magnetization and zero field cooling-field cooling (ZFC/FC) curves have been measured with a vibrating sample magnetometer (VSM) and parameters such as saturation magnetisation (M_S), remanent magnetization (M_r), coercivity (H_c) and blocking temperature (T_B) were obtained for all the DMSA-coated IONPs dispersed in water.

All samples show superparamagnetic behaviour at 250 K with negligible coercivity and remanent magnetisation. M_S values measured here are around 70 emu g^{-1} at 250 K and 73 emu g^{-1} at 5 K for IONPs with core sizes >10 nm (Table 3). These M_S values are higher than those often reported in the literature for IONPs synthesised by the same method, which are commonly below 60 emu g^{-1},[13,15] and sometimes even lower than 40 emu g^{-1}.[7,12,14] This result is especially relevant considering that M_S values were measured after transferring the particles to water, because some oxidation of magnetite to maghemite could take place at least at the surface.

Table 3 Properties of DMSA-coated IONPs dispersed in water

Entry	Label	Core size[a] (nm)	Hydrodynamic size[b] (nm)	M_S[c] (emu g^{-1}) 5 K /250 K
1	DMSA-IO-2	12 ± 1	49 (0.22)	71/66
2	DMSA-IO-8	14 ± 1	45 (0.15)	73/69
3	DMSA-IO-9	18 ± 2	66 (0.18)	73/70
4	DMSA-IO-10	22 ± 2	48 (0.17)	72/69

[a] Mean size and standard deviation as measured by TEM. [b] Hydrodynamic size and polydispersity index (in brackets) as obtained by DLS. [c] M_S measured from water dispersions and expressed per gram of γ-Fe_2O_3.

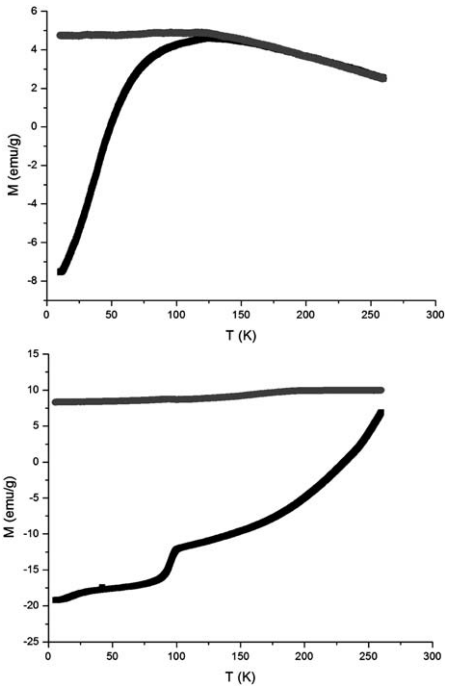

Fig. 5 Zero field cooling/field cooling (ZFC/FC) magnetization *versus* temperature curves of: DMSA-IO-1 (9 nm, up) and DMSA-IO-10 (22 nm, down). Black: ZFC, grey: FC.

M_S values for nanoparticles are expected to be smaller than those for bulk materials because of finite size effects and disorder at the surface.[34] Both effects become more important as the IONPs become smaller. The same trend is observed in the present work where M_S values are lower (50–60 emu g^{-1}) for the smallest nanoparticles (IO-1, IO-3 and IO-5; see Table S1†). Additionally lower M_S values have been observed for nanoparticles with broad size distributions (IO-6 and IO-7). This reduction of the M_S value can be explained to be the result of the presence of a significant fraction of nanoparticles with small size in IO-6 (see Fig. 1), whose contribution to the M_S value is much lower. This is also typical of IONPs prepared by coprecipitation, whose M_S values are around 50–60 emu g^{-1}.

For comparison, ZFC–FC curves of DMSA-IO-1 (9 nm) and DMSA-IO-10 (22 nm) are shown in Fig. 5 (all the ZFC–FC curves are displayed in Fig. S5†). The slope in the ZFC curves becomes smoother when the particle size increases. For the largest particles, IO-9 (18 nm) and IO-10 (22 nm), the Verwey transition, characteristic of magnetite (125 K),[35] is clearly observed at *ca.* 90–95 K, while for smaller particles it does not appear. This indicates a reduction of this temperature transition for small particle sizes,[36] or the oxidation of magnetite to maghemite in particles smaller than 18 nm, probably during the water transference process.[37]

Colloidal stability in biological buffers

The stability of the IONP dispersions has been studied measuring the changes in the hydrodynamic size (D_{HYD}) by DLS as a

function of the buffer concentration and nature (phosphate buffered saline solution, PBS, and sodium 2-[4-(2-hydroxyethyl)-1-piperazinyl]ethanesulfonate, HEPES), and nanoparticle size and concentration. Thus, an increase in D_{HYD} indicates that agglomeration has taken place and that the IONPs are losing stability. We have studied IONPs with core sizes (as measured by TEM) of 9, 12, 14, 15 and 18 nm, and dispersions with Fe concentrations (measured by ICP-OES) of 0.05, 0.1 and 0.5 g L^{-1}, which are typical concentrations for cell culture experiments. For a given size, the Fe concentration is proportional to the nanoparticle concentration.

Dispersions in water of DMSA-coated IONPs present long-term stability at room temperature (20–25 °C) or in the refrigerator (4 °C). Thus, after being stored at 4 °C for more than 10 months, no changes in the hydrodynamic size (as checked by DLS), the magnetic properties (as checked by VSM) or sedimentation were observed. However, the colloidal stability of the particles is expected to be affected in the presence of common buffers used in biological experiments.[15] One of the most common buffers in biology is the so-called phosphate buffered saline solution (PBS), which is a mixture of phosphates (typically MH_2PO_4 and M_2HPO_4, M = Na and/or K) and MCl salts in water, commonly with concentrations of 10.4 mM of phosphates (Na_2HPO_4: 7.7 mM, NaH_2PO_4: 2.7 mM) and 0.154 M of sodium and/or potassium chloride. For this work we have defined this concentration as *[PBS1x]*. We have used PBS only with M = Na to avoid effects due to the nature of the cations (since K and Na cations are different in ionic size and reactivity).

Influence of iron content and saline concentration. The behaviour of DMSA-coated IONPs of 8.9 nm dispersed in PBS buffer (concentration *[PBS1x]*) at three different iron concentrations (0.05, 0.1, and 0.5 g L^{-1} which correspond to 0.007, 0.014 and 0.07 wt% of magnetic iron oxide) is shown in Fig. 6. In all cases the hydrodynamic size increases with time, and this increase is more pronounced at higher iron concentrations (that is, at higher particle concentrations). Hence with 0.5 g L^{-1} of iron, the suspension is slightly turbid as soon as 1 h after the PBS addition and particles precipitate after 3 hours. With iron concentrations of 0.05 g L^{-1} and 0.1 g L^{-1} precipitation is only observed after more than 12 hours. As stated above, for IONPs of a given size, the nanoparticle concentration increases with the iron concentration; so these results indicate an enhanced stability for the less concentrated samples.

At lower PBS concentrations (*[PBS1x]*/2, *[PBS1x]*/4 and *[PBS1x]*/8) the stability of the DMSA-coated IONPs is dramatically increased (see Fig. 7). For example, with *[PBS1x]*/4 no precipitation was observed after 1 week, with an Fe concentration of 0.5 g L^{-1}, after 1 week (D_{HYD} < 100 nm). With an Fe concentration of 0.1 g L^{-1} the IONPs are even more stable and D_{HYD} is below 200 nm after 2 weeks (Fig. 7). With a higher buffer concentration, *[PBS1x]*/2, after one day at room temperature nanoparticles still displayed D_{HYD} < 200 nm. However, after 2 days, in both concentrations 0.1 and 0.5 g L^{-1}, D_{HYD} had a value of around 900 nm (not shown in Fig. 7) and precipitation of the particles began shortly after measurements.

These observed trends unambiguously indicate that stability is enhanced at low iron contents (low IONP concentration) and low salt concentrations in accordance with colloidal stabilization mechanisms based mainly on electrostatic repulsion. Thus, long-term storage of DMSA-coated IONPs in PBS buffer is possible only for low PBS and iron concentrations (<*[PBS1x]*/2 and <1 g L^{-1}, respectively). For biological studies requiring higher PBS

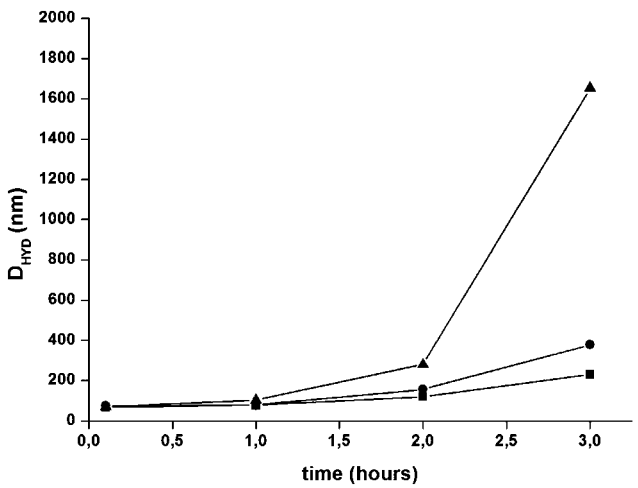

Fig. 6 Progress with time of the hydrodynamic size of IO-5 (core size = 8.9 nm) after adding PBS buffer (*[PBS1x]*) at room temperature, and iron concentrations of 0.05 (■), 0.1 (●) and 0.5 (▲) g L^{-1}.

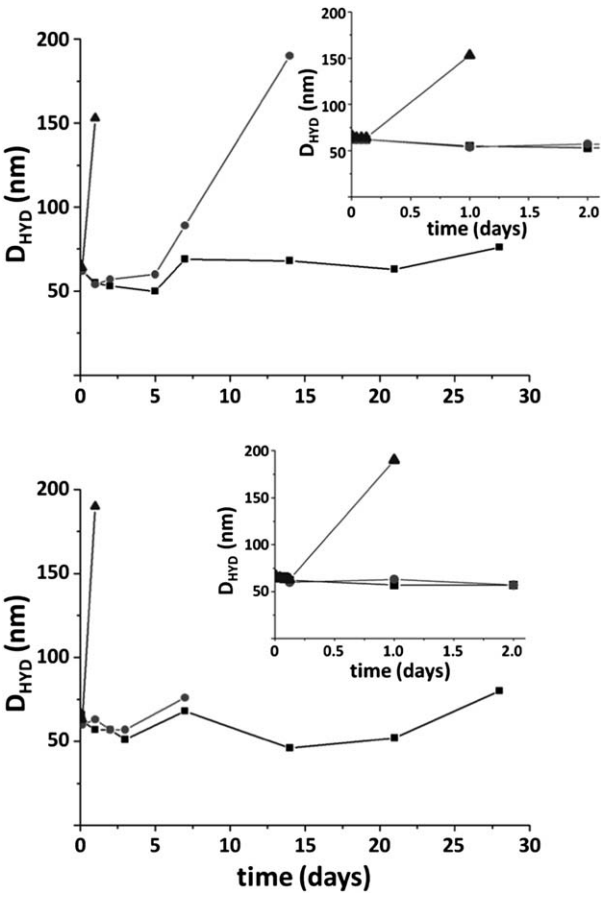

Fig. 7 Progress with time of the hydrodynamic size of DMSA-IO-5 (core size = 8.9 nm) at different PBS concentrations *[PBS1x]*/2 (▲), *[PBS1x]*/4 (●) and *[PBS1x]*/8 (■) and at different iron concentrations (up: 0.1 g L^{-1}, down: 0.5 g L^{-1}).

and iron concentrations, the best choice is to store the samples in pure water and to add the buffer few hours before the *in vitro* or *in vivo* experiments.

If HEPES is used instead of PBS, in the same conditions, no loss of stability is observed after several days. But, if NaCl (1.54 M) is added together with HEPES, then a behaviour similar to that with PBS is observed, suggesting that NaCl is playing an important role in the loss of colloidal stability. This point will be discussed below.

Influence of IONP size. The influence of the core size of the nanoparticles on colloidal stability in biological buffers has been also investigated using IONPs with core sizes of 12, 14, and 18 nm (DMSA-IO-2, DMSA-IO-8 and DMSA-IO-9 respectively). Data show that the stability is reduced when the size of the IONPs increases. With the buffer in concentration *[PBS1x]*, and with an iron content of 0.1 g L^{-1}, the nanoparticles display hydrodynamic sizes in the micrometer range after two hours in the case of DMSA-IO-2, and after a few minutes in the case of the larger DMSA-IO-8 and DMSA-IO-9 (which precipitate within one hour). Again, at lower buffer concentrations the stability is preserved, as is the case for sample DMSA-IO-2 with *[PBS1x]*/8 (D_{HYD} < 60 nm), which is stable for several weeks. Regarding the influence of the IONP size on the colloidal stability it is necessary to consider that, as the size of the particle increases, van der Waals forces become stronger, favouring aggregation.[38] In the same sense, attractive magnetic interaction driving to aggregation would be more important with larger IONPs (*i.e.* larger dipoles).

The main source of stabilization of DMSA-coated IONPs is the electronic repulsion between IONPs, which are negatively charged.[39] DMSA is a small molecule that confers little steric stabilization if compared with typical polymers used as stabilizers, *e.g.* dextran and polyethylene glycol derivatives. A plausible hypothesis for the origin of the loss of colloidal stability in PBS buffer is the surface charge shielding of the IONPs by the ions of the buffer. This hypothesis has been tested with DMSA-IO-8 and DMSA-IO-9 in two sets of experiments: one with the IONPs in the presence of phosphates in the same concentration as *[PBS1x]* (Na_2HPO_4: 7.7 mM, NaH_2PO_4: 2.7 mM) but without NaCl, and the other with the same concentration of NaCl (0.154 M) but without phosphates. In the first case, only with phosphates, the nanoparticles are very stable, with hydrodynamic sizes below 200 nm after several weeks at room temperature, even with the highest concentration of nanoparticles (0.5 g L^{-1} of Fe). By contrast, if only NaCl (1.54 M) is added, without phosphates, results are similar than when using *[PBS1x]*, and hydrodynamic sizes are in the micron range in a short time after adding the buffer.

Our data confirm that the loss of stabilization in DMSA-coated IONPs is mainly due to the shielding of the surface charge caused by the NaCl and that the phosphates cause almost no loss of stability. These results differ from previous reports in the literature in which IONPs coated with poly(acrylic acid) (PAA), polyethylenimine (PEI) and glutathione (GSH) exhibited higher stabilities against NaCl than against PBS.[15] With PAA, PEI and GSH coatings the stabilization is mainly steric, in contrast to the DMSA employed in this work, which provides a predominantly electrostatic stabilization.

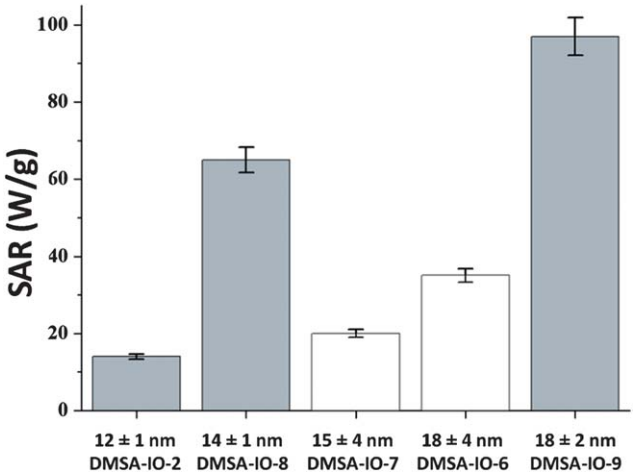

Fig. 8 SAR values obtained for IONPs with different sizes and with narrow and broad size distributions (grey and white respectively) when exposed to the same H_{AC} conditions (50 mT and 77 kHz).

Magneto-thermal properties under alternating magnetic fields

As stated in the introduction, IONPs are potential heating mediators for cancer treatment through hyperthermia.[22] In order to evaluate the influence of the structural and magnetic properties of IONPs on the heat dissipation power when subjected to H_{AC}, we measured the SAR values of IONPs with different sizes, size distributions and M_S values. Data are highly reproducible even after applying H_{AC} for hours over the same sample. This is due to the high colloidal stability of the DMSA-coated IONPs dispersed in water that do not precipitate even under these harsh conditions. Fig. 8 shows the SAR values obtained for IONPs synthesized in different ways. The SAR value progressively rises with the IONP size for narrow size distributions (DMSA-IO-2, -8 and -9). For IONPs of similar average size, the SAR value significantly increases, as does the M_S value (Table S1†), when the size distribution becomes narrower. Thus, the SAR value is more than 3 times higher for DMSA-IO-8 (mean size of 14 nm and narrow size distribution; SAR = 65 W g^{-1}) if compared with DMSA-IO-7 (mean size of 15 nm but broad size distribution; SAR = 20 W g^{-1}). In a similar manner, for IONPs with the same mean size of 18 nm but different size distributions, the SAR changes from 35 W g^{-1} with the IONPs with the broader size distribution (DMSA-IO-6) to 97 W g^{-1} for the narrower one (DMSA-IO-9). This can be explained in a similar way as for the increase of the M_S value: narrower size distribution implies a lower amount of IONPs with smaller size and, therefore, a higher dissipation power associated with the IONPs with larger size, which dominates the thermal properties of the IONP sample. This correlation between SAR and size distribution has been previously suggested,[22] and our results allow its quantification.

Conclusions

In this work, we have shown that the high temperature decomposition of an iron oleate complex can be used to obtain superparamagnetic nanocrystals with sizes over 10 nm that display high saturation magnetization values. A reaction procedure has been established to synthesize IONPs with sizes over 20 nm with

narrow size distribution and high magnetization values. Results concerning the size of the IONPs as a function of the oleic acid added to the reaction medium show a complex behaviour that can be qualitatively explained in terms of nucleation and growth rates. Broader size distributions lead to worse magnetic properties either in large (15 or 18 nm) or in small IONPs (9 nm).

After surface modification, DMSA-coated IONPs display a great stability in water, making it possible to store them for more than one year at 4 °C without significant losses in terms of structural, colloidal and magnetic properties. Three factors have been identified to affect the stability of DMSA-coated IONPs dispersed in buffers: size of the nanoparticles, concentration of the IONPs and concentration of NaCl present in common buffers. For biological applications, these three factors should be considered to avoid colloidal stability issues. These results lead us to conclude that the best way to use them in biological buffers containing NaCl, like PBS, is to add the buffer within few hours before the subsequent application. If it is necessary, long-term storage in buffers is possible without affecting too much the stability with low concentrations of particles and salts.

We have experimentally shown the influence of the size and the size distribution on the magnetic and magneto-thermal properties of IONPs. Our results highlight the importance of narrow size distributions and high saturation magnetization values. The synthesis conditions studied here provide a valuable knowledge to obtain IONPs with improved colloidal, magnetic and magneto-thermal properties to be used as intracellular hyperthermia mediators or in other biomedical applications.

Acknowledgements

The authors thank Isabel Sobrados and Virginia Díez (ICMM-CSIC) for the NMR characterization. This work has been partially supported by EU-FP7 MULTIFUN project (no. 262943), Spanish Ministry of Economy and Competitiveness (MAT2011-23641, MAT2010-21822-C02-01), Consolider-Ingenio en Nanociencia Molecular (CSD2007-00010) and NANOBIOMAGNET project funded by Comunidad de Madrid (S2009/MAT-1726). FJT acknowledges financial support from Ramon y Cajal (RYC-2011-09617) subprogram.

Notes and references

1 P. Tartaj, M. P. Morales, T. Gonzalez-Carreño, S. Veintemillas-Verdaguer and C. J. Serna, *Adv. Mater.*, 2011, **23**, 5243.
2 V. L. Kolesnichenko, Synthesis of Nanoparticulate Magnetic Materials, in *Magnetic Nanoparticles*, S. P. Gubin, ed., Wiley-VCH Verlag GmbH & Co. KGaA, Weinheim, 2009, ch. 2, pp. 25–58.
3 (*a*) J. Park, E. Lee, N.-M. Hwang, M. Kang, S. C. Kim, Y. Hwang, J.-G. Park, H.-J. Noh, J.-Y. Kim, J.-H. Park and T. Hyeon, *Angew. Chem., Int. Ed.*, 2005, **44**, 2873; (*b*) T. Hyeon, S. S. Lee, J. Park, Y. Chung and H. B. Na, *J. Am. Chem. Soc.*, 2001, **123**, 12798.
4 S. Sun and H. Zeng, *J. Am. Chem. Soc.*, 2002, **124**, 8204.
5 J. Cheon, N.-J. Kang, S.-M. Lee, J.-H. Lee, J.-H. Yoon and S. J. Oh, *J. Am. Chem. Soc.*, 2004, **126**, 1950.
6 W. W. Yu, J. C. Falkner, C. T. Yavuz and V. L. Colvin, *Chem. Commun.*, 2004, 2306.
7 J. Park, K. An, Y. Hwang, J.-G. Park, H.-J. Noh, J.-Y. Kim, J.-H. Park, N.-M. Hwang and T. Hyeon, *Nat. Mater.*, 2004, **3**, 891.
8 M. Levy, A. Quarta, A. Espinosa, A. Figuerola, C. Wilhelm, M. García-Hernández, A. Genovese, A. Falqui, D. Alloyeau, R. Buonsanti, P. D. Cozzoli, M. A. García, F. Gazeau and T. Pellegrino, *Chem. Mater.*, 2011, **23**, 4170.
9 S. Palchoudhury, W. An, Y. Xu, Y. Qin, Z. Zhang, N. Chopra, R. A. Holler, C. H. Turner and Y. Bao, *Nano Lett.*, 2011, **11**, 1141.
10 L. M. Bronstein, X. Huang, J. Retrum, A. Schmucker, M. Pink, B. D. Stein and B. Dragnea, *Chem. Mater.*, 2007, **19**, 3624.
11 L. M. Bronstein, J. E. Atkinson, A. G. Malyutin, F. Kidwai, B. D. Stein, D. G. Morgan, J. M. Perry and J. A. Karty, *Langmuir*, 2011, **27**, 3044.
12 S. G. Kwon, Y. Piao, J. Park, S. Angappane, Y. Jo, N.-M. Hwang, J.-G. Park and T. Hyeon, *J. Am. Chem. Soc.*, 2007, **129**, 12571.
13 N. Bao, L. Shen, Y. Wang, P. Padhan and A. Gupta, *J. Am. Chem. Soc.*, 2007, **129**, 12374.
14 A. Shavel, B. Rodríguez-González, J. Pacifico, M. Spasova, M. Farle and L. M. Liz-Marzán, *Chem. Mater.*, 2009, **21**, 1326.
15 Y. Xu, Y. Qin, S. Palchoudhury and Y. Bao, *Langmuir*, 2011, **27**, 8990.
16 Y. Hou, Z. Xu and S. Sun, *Angew. Chem., Int. Ed.*, 2007, **46**, 6329.
17 B. P. Pichon, O. Gerber, C. Lefevre, I. Florea, S. Fleutot, W. Baaziz, M. Pauly, M. Ohlmann, C. Ulhaq, O. Ersen, V. Pierron-Bohnes, P. Panissod, M. Drillon and S. Begin-Colin, *Chem. Mater.*, 2011, **23**, 2886.
18 K. M. Krishnan, *IEEE Trans. Magn.*, 2010, **46**, 2523.
19 A. Villanueva, M. Cañete, A. G. Roca, M. Calero, S. Veintemillas-Verdaguer, C. J. Serna, M. P. Morales and R. Miranda, *Nanotechnology*, 2009, **20**, 115103.
20 R. Mejías, S. Pérez-Yagüe, A. G. Roca, N. Pérez, Á. Villanueva, M. Cañete, S. Mañes, J. Ruiz-Cabello, M. Benito, A. Labarta, X. Batlle, S. Veintemillas-Verdaguer, M. P. Morales, D. F. Barber and C. J. Serna, *Nanomedicine*, 2010, **5**, 397.
21 R. Mejías, S. Pérez-Yagüe, L. Gutiérrez, L. I. Cabrera, R. Spada, P. Acedo, C. J. Serna, F. J. Lázaro, A. Villanueva, M. P. Morales and D. F. Barber, *Biomaterials*, 2011, **32**, 2938.
22 A. Jordan, P. Wust, H. Fähling, W. John, A. Hinz and R. Felix, *Int. J. Hyperthermia*, 1993, **9**, 51.
23 (*a*) Q. A. Pankhurst, J. Connolly, S. K. Jones and J. Dobson, *J. Phys. D: Appl. Phys.*, 2003, **36**, R167; (*b*) Q. A. Pankhurst, N. K. T. Thanh, S. K. Jones and J. Dobson, *J. Phys. D: Appl. Phys.*, 2009, **42**, 224001.
24 F. J. Teran, C. Casado, N. Mikuszeit, G. Salas, A. Bollero, M. P. Morales, J. Camarero and R. Miranda, *Appl. Phys. Lett.*, 2012, **101**, 062413.
25 K. Nakamoto, *Infrared and Raman Spectra of Inorganic and Coordination Compounds, Part B, Applications in Coordination, Organometallic, and Bioinorganic Chemistry*. John Wiley & Sons, Inc, 6th edn, 2009.
26 P. Conte, R. Spaccini and A. Piccolo, *Prog. Nucl. Magn. Reson. Spectrosc.*, 2004, **44**, 215.
27 J. M. Vargas and R. D. Zysler, *Nanotechnology*, 2005, **16**, 1474.
28 C. J. Meledandri, J. K. Stolarczyk, S. Ghosh and D. F. Brougham, *Langmuir*, 2008, **24**, 14159.
29 V. K. LaMer and R. H. Dinegar, *J. Am. Chem. Soc.*, 1950, **72**, 4847.
30 Z. L. Wang, *J. Phys. Chem. B*, 2000, **104**, 1153.
31 X. Peng, J. Wickham and A. P. Alivisatos, *J. Am. Chem. Soc.*, 1998, **120**, 5343.
32 N. Fauconnier, J. Pons, J. Roger and A. Bee, *J. Colloid Interface Sci.*, 1997, **194**, 427.
33 It is worth noting that the last step (sterilization) is not necessary if the nanoparticles are not going to be used for biological purposes.
34 (*a*) X. Batlle and A. Labarta, *J. Phys. D: Appl. Phys.*, 2002, **35**, R15; (*b*) X. Batlle, N. Pérez, P. Guardia, O. Iglesias, A. Labarta, F. Bartolomé, L. M. García, J. Bartolomé, A. G. Roca, M. P. Morales and C. J. Serna, *J. Appl. Phys.*, 2011, **109**, 07B524.
35 F. Walz, *J. Phys.: Condens. Matter*, 2002, **14**, R285.
36 G. F. Goya, T. S. Berquó, F. C. Fonseca and M. P. Morales, *J. Appl. Phys.*, 2003, **94**, 3520.
37 R. Aragon, J. Buttrey, J. P. Shepherd and J. M. Honig, *Phys. Rev. B: Condens. Matter Mater. Phys.*, 1985, **31**, 430.
38 Y. Lalatonne, J. Richardi and M. P. Pileni, *Nat. Mater.*, 2004, **3**, 121.
39 A. G. Roca, S. Veintemillas-Verdaguer, M. Port, C. Robic, C. J. Serna and M. P. Morales, *J. Phys. Chem. B*, 2009, **113**, 7033.